Numerical Study of Flow around Twin Cubic Obstacles Issued from a Bent Chimney

I. **Bhouri Baouab, N. Mahjoub Said, H.Mhiri, G. Le Palec, P. Bournot**

Abstract—we present in this work a numerical study of pollutant dispersion resulting from a bent chimney around twin obstacles placed in the lee side of the source.

A three-dimensional numerical model with the turbulent Reynolds Stress Model (RSM) and a non-uniform grid system was used to examine the effects of a double tandem obstacle cubic on the development of the incoming flow.

The results obtained in three-dimensional configuration make possible the description of the dynamic and masses features and the determination of the velocity ratio effect on the pollutant distribution.

Index Terms—bent chimney, two cubic, numerical simulations, dynamic feature, mass feature

I. INTRODUCTION

The increased concentrations of atmospheric pollutants observed in urban areas and the concern that has been developed for the effects of pollution on human health have increased the need for thorough studies of atmospheric flow and dispersion near buildings. We will restrain in the present study to the works that considered two obstacles.

Oke [1] studied in a wind tunnel the flow in a street bordered by two obstacles, and showed the existence of three modes depending on the dimension of the obstacles and the distance that separates them. If the obstacles are well spaced from/to each other, the flow is connected with a succession of identical structures around insulated obstacles. When the variation decreases, the wakes are disturbed. The flow downstream from an obstacle is reinforced by a deflection on the level of the face upstream of the following obstacle. When the ratio between the distance separating the obstacles and their height is even weaker, the street is closed again and a recirculation is established with one street identical to the other. The flow is then known as razing.

Martinuzzi [2000] studied the flow past two cubes in tandem, it was observed that for Reynolds numbers in the range $3000 < Re < 40,000$ the flow around the cubes is only weakly sensitive to Reynolds number. In particular, their detailed measurements at $Re = 22,000$ are considered to be representative for all Reynolds numbers in the range $12,000 < Re < 40,000$. Through a series of experiments for a wide range of cube spacing, they observed that depending on the distance between the cubes three distinct flow patterns exist. For small spacing, the shear layer separating from the first cube reattaches on the sides of the second obstacle and Periodic vortex shedding can only be detected in the wake of the downstream cube. The two cubes essentially act as a single bluff body.

In the work of Martinuzzi [3] two surface-mounted cubes, of height h, in tandem arrangement was investigated for a spacing 2h using phase-averaged Laser Doppler Velocimetry. Tests were conducted for a Reynolds number of 22,000, based on h and the free stream velocity, and an approximately 0.07h thick laminar boundary layer. They showed that the structure of the turbulent field in the cavity region differs significantly from that in the base region of a two-dimensional obstacle.

Norio [4] studied the flow around two circular cylinders in tandem arrangement using a third-order upwind finite element scheme. The two circular cylinders are arranged with some spacing between the cylinders. At the Reynolds number of 1000, the obtained numerical results are qualitatively compared with experimental data.

Mahjoub [5] described the investigation on the flow around circular cylinder obstacles mounted on a ground floor. They used the Particle Image Velocimetry (PIV) technique. They showed that the size of the vortex at the leeside of the cylinder is big; the turbulence intensity is, however, stronger.

In parallel to the experiments a three-dimensional numerical model which employs a RMS turbulence closure scheme and a won-uniform grid system was developed. They examined the wind flow perturbations, recirculation and turbulence generated by two circular cylinder obstacles on tandem arrangements. They showed that the flow reattachment promoted by the upwind obstacle acted to

restrict the vertical extent of vortex below the roof-level. Ultimately, it enlarged recirculation zone behind the second obstacle and reduced the vertical velocity and average height of flow above the downwind cylinder as well as in the downwind. An experimental investigation was carried out by Mahjoub[6] to study the structure of the flow field around three dimensional rectangular obstacles. The study was performed in wind tunnel using a Particle Image Velocimetry (PIV) system. They showed that the structure of the flow depend on the spacing between a pair of tandem aligned obstacles.

A three-dimensional numerical model with the turbulent Reynolds Stress Model (RSM) and a non-uniform grid system was used to examine the effects of a single rectangular obstacle and a double tandem obstacle on the development of the incoming flow. For the case of two rectangular tandem obstacles, the flow patterns were characterized in the gap region as a function of the distance between the obstacles.

Joongcheol Paik et al [7] investigated the performance of unsteady Reynolds-averaged Navier–Stokes (URANS) computation and various versions of detached eddy simulation (DES) in resolving coherent structures in turbulent flow around two cubes mounted in tandem on a flat plate at Reynolds number (*Re*) of 22,000 and for a thin incoming boundary layer. Calculations are carried out using four different coherent structure resolving turbulence models: [8] URANS; [9] the standard DES [10] the Delayed DES (DDES); and [11] the DES. The grid sensitivity of the computed solutions is examined by carrying out simulations on two successively refined grids.

They showed that all turbulence models reproduce essentially identical separation of the approach thin boundary layer and yield an unsteady horseshoe vortex system consisting of multiple vortices in the leading edge region of the upstream cube.

However they observed some discrepancies between the URANS and all DES solutions in other regions of interest such as the shear layers emanating from the cubes, the inter-cube gap and the downstream wake.

II. NUMERICAL STUDY

The mean flow field surrounding chimney and obstacles attached to a wall under a turbulent flow is obtained by varying u_∞. Consideration is given to a steady, three-dimensional and turbulent flow. The studied model is shown in fig. 1. We consider a reel case: the height of the chimney is 85m, the diameter is 8.5m and the length of the bent is 10m. Twin similar cubic obstacles were placed downstream of the bent chimney.
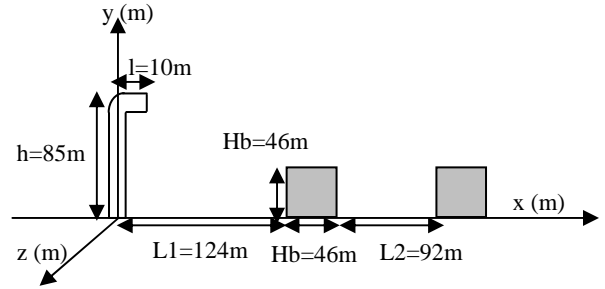

Fig. 1 Model configuration

The equations governing this problem are obtained using the Favre decomposition and are thus written in the following form:

$$\frac{\partial(\overline{\rho}\tilde{u}_i)}{\partial x_i} = 0 \qquad (1)$$

$$\frac{\partial\left(\overline{\rho}\tilde{u}_i\tilde{u}_j\right)}{\partial x_j} = -\frac{\partial\overline{p}}{\partial x_i} + \frac{\partial}{\partial x_j}\left(\mu\frac{\partial\tilde{u}_i}{\partial x_j} - \overline{\rho u_i'' u_j''}\right) + \left(\overline{\rho}_\infty - \overline{\rho}\right)g\delta_{ij} \qquad (2)$$

$$\frac{\partial\left(\overline{\rho}\tilde{u}_j\tilde{T}\right)}{\partial x_j} = \frac{\partial}{\partial x_j}\left[\left(\frac{\mu}{Pr} + \frac{\mu_t}{\sigma_t}\right)\frac{\partial\tilde{T}}{\partial x_j}\right] \qquad (3)$$

$$\frac{\partial\left(\overline{\rho}\tilde{u}_j\tilde{f}\right)}{\partial x_j} = \frac{\partial}{\partial x_j}\left[\left(\frac{\mu}{Sc} + \frac{\mu_t}{\sigma_f}\right)\frac{\partial\tilde{f}}{\partial x_j}\right] \qquad (4)$$

The introduction of the fluctuating sizes makes this system open. Its closing requires the use of a turbulence model which makes it possible to obtain a number of equations equal to the number of Unknown parameters.

Mahjoub et al. [12] show that the three first-order models (the standard k-ε model, the k-ε RNG Model, and the realizable k-ε model) produce identical results in the upstream and far downstream regions of the three-dimensional jet. However, only the second order model is shown to give good results in the exit region and in the trailing zone of the jet. Based on this last result, we choose this second-order closure model (also called Reynolds Stress Model) in this paper. So the following equation is solved:

$$\underbrace{\frac{\partial}{\partial x_k}(\overline{\rho}\tilde{u}_k\overline{u_i''u_j''})}_{C_{ij}} = \underbrace{\frac{\partial}{\partial x_k}\mu\frac{\partial}{\partial x_k}(\overline{u_i''u_j''})}_{D_{ij}^L} \underbrace{-\overline{\rho}\left[\overline{u_i''u_k''}\frac{\partial\tilde{u}_j}{\partial x_k} + \overline{u_j''u_k''}\frac{\partial\tilde{u}_i}{\partial x_k}\right]}_{P_{ij}} + D_{ij}^T + G_{ij} + \phi_{ij} + \varepsilon_{ij} \qquad (5)$$

C_{ij} being the convective term. D_{ij}^L, P_{ij}, D_{ij}^T, G_{ij}, ϕ_{ij} and ε_{ij} are, respectively, the molecular diffusion, the stress

Production, the turbulent diffusion, the buoyancy production, the pressure strain and the dissipation rate [13].

The equations of the turbulent kinetic energy (k) and of the dissipation rate of the kinetic energy (ε) associated with the second-order model are defined as follows:

$$\frac{\partial \left(\bar{\rho} \tilde{u}_j k \right)}{\partial x_j} = \frac{\partial}{\partial x_j} \left[\left(\mu + \frac{\mu_t}{\sigma_k} \right) \frac{\partial k}{\partial x_j} \right] + \frac{1}{2} \left(P_{ii} + G_{ii} \right) - \bar{\rho} \, \varepsilon \qquad (6)$$

$$\frac{\partial \left(\bar{\rho} \tilde{u}_j \varepsilon \right)}{\partial x_j} = \frac{\partial}{\partial x_j} \left[\left(\mu + \frac{\mu_t}{\sigma_\varepsilon} \right) \frac{\partial \varepsilon}{\partial x_j} \right] + C_{\varepsilon 1} \frac{1}{2} \left(P_{ii} + C_{\varepsilon 3} G_{ii} \right) \frac{\varepsilon}{k} - C_{\varepsilon 2} \, \bar{\rho} \, \frac{\varepsilon^2}{k} \qquad (7)$$

The boundary conditions associated with the above system of differential equations are summarised in table1.

Table 1. Boundaries conditions

	U	T	f	k	ε
chimney	$\tilde{u} = U$ $\tilde{v} = 0$ $\tilde{w} = 0$	$\tilde{T} = T_0$	$\tilde{f}_m = f_{0\,m}$	$k_0 = 10^{-3} v_0$	$\varepsilon = \frac{k_0^{3/2}}{0.5 d}$
Crossflow	$\tilde{u} = u_\infty$ $\tilde{v} = 0$ $\tilde{w} = 0$	$\tilde{T} = T_\infty$	$\tilde{f}_m = 0$	$k_\infty = 5.10^{-3} u_\infty$	$\varepsilon = \frac{k_\infty^{3/2}}{0.2 H}$
Obstacles and ground	$\tilde{u} = 0$ $\tilde{v} = 0$ $\tilde{w} = 0$	$\frac{\partial \tilde{T}}{\partial n} = 0$	$\frac{\partial \tilde{f}_m}{\partial n} = 0$	$k = 0$	$\frac{\partial \varepsilon}{\partial y} = 0$

Several important problems arise from the numerical simulation of this problem. The topology of the flow requires a very fine meshing in a great part of the domain. In order to get a precise description of any variations, particularly near the chimney and the obstacles, we adopted a non-uniform meshing.

The numerical code uses the finite volume method, the solution of equations being based on the algorithm SIMPLER proposed by Patankar [14] for the obtained algebraic equations we use an implicit scheme. The elimination method of Gauss associated with an under-relaxation technique is used to solve the resulting tridiagonal matrix.

We introduce a temperature gradient between the two flow and we inject a non reacting fume mixed with air within the chimney nozzles. The composition of the smoke is 20.9% CO_2, 76.9% N_2, 1.8% O_2, and 0.4 % SO_2. The ejection velocity UO=4m/s, the temperature of ejection T0=120° and a wind velocity U∞=18°, the cross flow temperature T∞=18°.

It is assumed that all species have the same mass fraction behaviour in this way; we will consider the CO_2 as a reference.
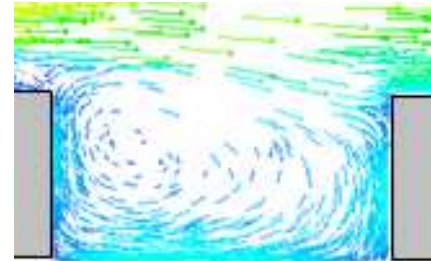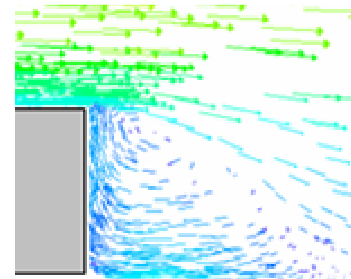
III. RESULTS

A. Dynamic features

We present in figure 2 mean velocity vector issued from a bent chimney around twin cubic obstacles under velocity ratio R=1.
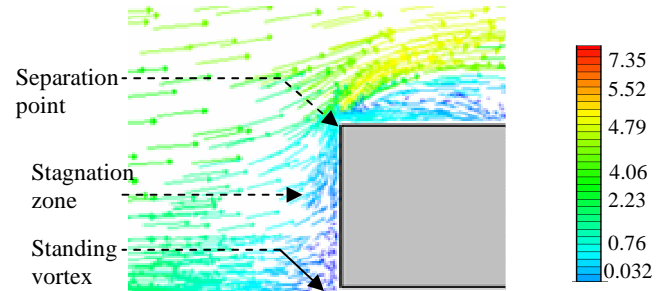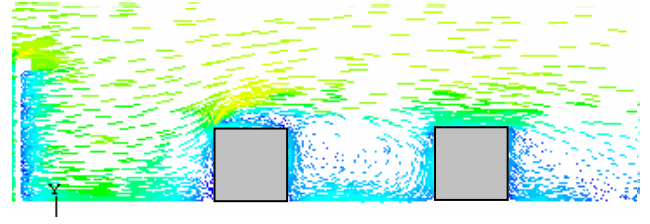
(a) Upstream of the first building

(b) Between the to building

(c) Downstream of the second building

Fig. 2 Global and zoomed views of the velocity vectors in the symmetry plan (z=0) at u₀=4m/s and u∞=4m/s.

Once the pollutant interacts with the buildings, the flow becomes disturbed and we distinguish four main zones:

The impact of the flow with the first bloc forces it to come back which generates a reverse flow region in the first zone.

The second zone is located above the first bloc. In fact the brutal increase of the pressure caused by the first bloc provokes the deviation of the fluid towards the roof of the met building.

The third zone is situated between the two obstacles. In this region we notice the existence of a large zone of recirculation.

The fourth zone is the region downstream the second bloc. This zone is generated by the effect of the second building.

Figure 2.a shows that the separation vector impinges on the front face of the first obstacle at a stagnation point. The

resulting recirculation gives rise to a horseshoe vortex, which extends to the sides of the obstacle. The position of the horseshoe vortex is shown upstream of the first obstacle.

We notice also that the flow is separated and accelerated when impacting against the first obstacle. We notice the development of the shear layer from the frontal corner.

The shear layer vortices (SLV) form at the interface between the front surface of the obstacle and the oncoming cross flow. They are the dominant structure in the region separating the bent chimney and the first building. These vortices are quasi-steady and form on the lateral edges of the obstacle as a result of the Kelvin-Helmholtz instability.

We can observe a well-developed vortex upstream of the model, with a stagnation point. This vortex is due to the shear of the approach flow near the floor.

Figure 2 b shows that between the two obstacles the main vortex centre is shifted towards the downstream obstacle side, the flow direction close to the floor being from the downstream to the upstream obstacle, while it is elongated along the horizontal direction we can also note the presence of the recirculation region developed above the obstacles. We assist to the development of significant clockwise vortices inside the space separating the twin obstacles.

In the wake of the downstream obstacle (Figure 2.c) a recirculation zone extends up to a distance of about 1h.

We present in figure 3 the contours of the longitudinal, vertical and lateral velocity components in the plan y=46m under a velocity ratio R=1.

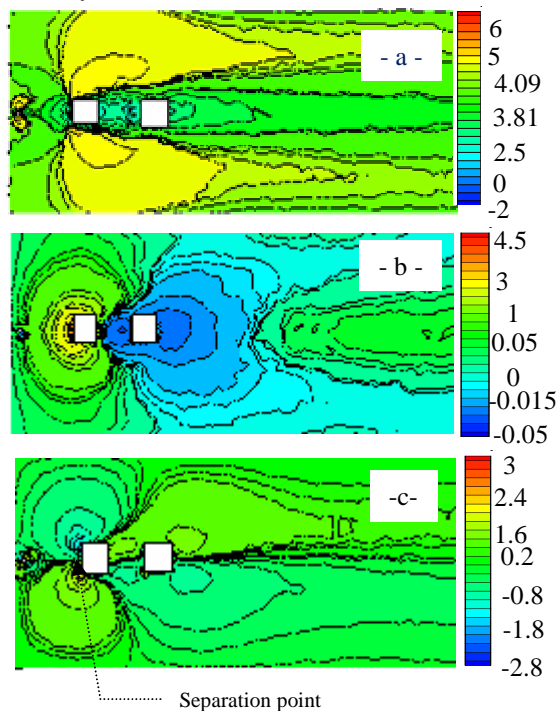

Figure 3.Contours of the velocity in the plan y=46 m
(a) Longitudinal velocity
(b) Vertical velocity
(c) Lateral velocity

Figure 3.a describes the horseshoe vortices (HSV) that form near the wall, windward of the first obstacle and wrap around the base of the building' columns.

The adverse pressure gradient formed at the injection wall forces the wall boundary layer to separate and form the horseshoe vortex. This vortex system is then stretched and convected about the periphery of the buildings like a necklace; this is analogous to the vortex system formed when an approaching boundary layer interacts with a cylinder mounted to a wall [15]. The HSV are found to be steady, oscillating or coalescing. Frequencies of oscillation have been found to be correlated with periodic motions of upright vortices. (Mariotti et al. [16]).

Figure 3.b describes the region wake.

Figure 3.c presents the separation point.

B. Masses features

Figure 4 presents the contours of the mass fraction of CO_2 under velocity ratio R=2 in the symmetry plan z=0. We notice that the pollutant ejected by the bent chimney tends to follow the shape of the first obstacle: in fact the fume circumvents the obstacle creating a recirculation zone. The trajectory of the obstacle is influenced by the flow around the first obstacle, by the recirculation zone, the wakes and the turbulence created in these regions. The second obstacle increases the disruption of the structure of the pollutant.
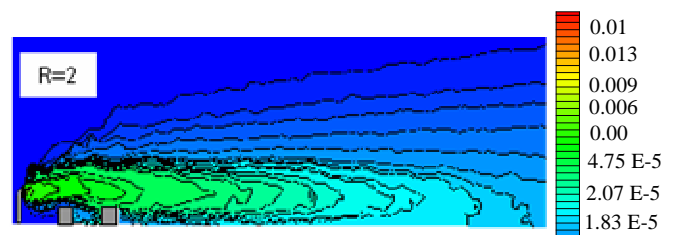

Figure 4.contours of mass fraction of CO_2 in symmetry plan Z=0 for R=2

We represent in figure 5 the vertical distribution of the mass fraction field under velocity ratio R=1 and R=2 in the symmetry plan (Z=0).

Figure 5 examine the vertical distribution of the mass fraction field under velocity ratio R=1 and R=2 at different longitudinal locations from the domain. These locations definitions are only based upon the buildings emplacement. The first position corresponds to the upstream of the first obstacle (x=90m), the second is placed at the roof of the first building (x=137m), the third is located between the two obstacles, the fourth one is situated at the roof of the second building (x=280m) and the last one is located far downstream by the end of the domain (x=400m).

Figure 5.a shows that at x=90m the mass fraction distribution adopts Gaussian profile behaviour as we assist to the registration of a single peak that is located at y=87m, it corresponds to the exit of the chimney. As we progress in the longitudinal direction (the fume direction) the initially Gaussian profile begins to widen: it expands in the vertical direction due to the altercations of the fume direction by the presence of the twin obstacles. The initial value is also affected due to the already began dispersion of the fume and in some cases its deposition downward.
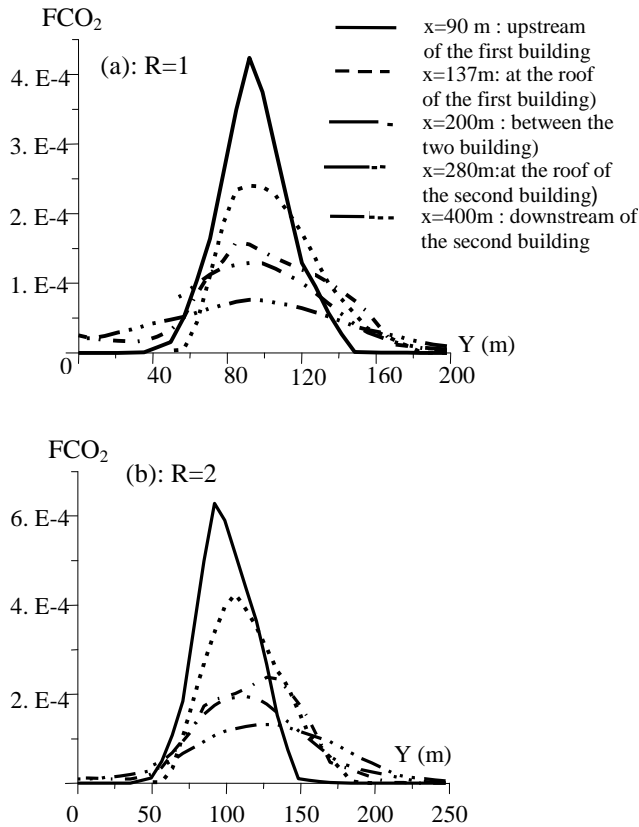
Figure5. Vertical distribution of the CO_2 mass fraction under two wind velocity in the symmetry plane (z=0)

Far downstream of the twin obstacles, the distribution of the CO_2 is progressively flattened: the distorting effect of the obstacles is no longer as significant as previously.

Figure 5.b shows that when the velocity ratio increases the mass fraction maximum moves to the top of the considered sections, and the maximum value increases also.

We concluded that wind velocity can greatly affect the pollutant concentration in a local area. The higher the wind speed, the lower the pollutant concentration. Wind dilutes pollutants and rapidly disperses them throughout the immediate area.

IV. CONCLUSION

We have examined in this paper the dynamic feature and the mass transfer generated under the presence of two similar cubic obstacles inline with a bent chimney. This study has been conducted numerically by the introduction of the finite volume method together with a turbulent closure model. The modelling of the resulting flowfield is based upon the resolution of the Nervier Stokes equations by means of the RSM turbulent model.

In this work we have described the dynamic and the turbulent field generated by the interaction of the flow ejected by a bent chimney with an oncoming cross flow in presence of twin cubic obstacles. We have concluded that once the pollutant interacts with the buildings, the flow becomes disturbed and we distinguish four main zones.

In the other hand we studied the mass transfer under two velocity ratios (R=1 and R=2). We deduced that the velocity ratio can greatly affect the pollutant concentration in a local area. The higher the wind speed, the lower the pollutant concentration.

V.NOMENCLATURE

Symbol	Description	Unit
d	Chimney Diameter	m
Hb	Building Height	m
f	Mass Fraction	No unit
g	Gravitational Acceleration	m/s^2
G_k	Term of production due to buoyancy forces	$kg/(m\ s^3)$
k	Kinetic Energy of Turbulence	m^2/s^2
$L2$	Distance separating the two buildings	m
P_k	Term of production due to the mean gradients	$kg/(m\ s^3)$
R	Velocity Ratio	No unit
S_{ij}	Mean Strain Rate	No unit
T	Temperature	K
U_∞	Crossflow Velocity	m/s
U_0	Injection Velocity	m/s
u_i, u_j	Velocity components along the i and j directions	
u, v, w	Velocity components along x, y, and z directions	m/s
x, y, z	Cartesian Coordinates	m
Greek Symbols		
ρ	Volume mass	Kg/m^3
β	Thermal Expansion Coefficient	No unit
ε	Dissipation Rate of the Turbulent Kinetic energy	No unit
μ	Kinetic Viscosity	$kg/(m\ s)$
μ_t	Turbulent (or eddy) Viscosity	$kg/(m\ s)$
δ_{ij}	Kronecker symbol (=1 if i=j and 0 if i≠j)	No Unit
Subscripts		
∞	Conditions in Crossflow	No unit
0	Exit Section of the	No unit
Superscripts		
$^-$	Reynolds average	No unit
$^\sim$	Favre average	No unit

REFERENCES

[1] Oke, T. R. (1988). Street design and urban canopy layer climate. Energy and Buildings, 11, 103-113.

[2] Martinuzzi and B. Havel, Turbulent flow around two interfering surface-mounted cubic obstacles in tandem arrangement, *ASME J. Fluid Engineering* 122, 2000, 24-31.

[3] Martinuzzi, R., J. and Havel B. (2004). Vortex shedding from two surface-mounted cubes in tandem. International Journal of Heat and Fluid Flow 25, 364–372.

[4] Norio Kondo, Daisuke Matsukuma Numerical simulation for flow around two circular cylinders in tandem. *International Journal of Computational Fluid Dynamics*, Vol. 19, No. 4. (May 2005), pp. 277-288.

[5]   N. Mahjoub, Three-dimensional experimental and numerical modelling of flow behaviour near wake circular. cylinder*,. Journal of Wind Engineering & Industrial Aerodynamics*

[6]   N. Mahjoub, Wind tunnel investigation and numerical simulation of the near wake dynamics for rectangular obstacles, Environmental Engineering Science Manuscript Central:EES-2007-0169 M. Young, The Techincal Writers Handbook. Mill Valley, CA: University Science, 1989.

[7]   R1Joongcheol Paika, Fotis Sotiropoulosb , and Fernando Porté-Agelb, "Detached eddy simulation of flow around two wall-mounted cubes in tandem," International Journal of Heat and Fluid Flow, Volume 30, Issue 2,2009, Pages 286-305J.

[8]   Spalart and Allmaras, 1994, A one-equation turbulence model for aerodynamic flows, La Recherche Aerospatiale 1 (1994), pp. 5–21

[9]   Spalart et al., 1997 P.R. Spalart, W.H. Jou, M. Strelets and S.R. Allmaras, Comments on the feasibility of LES for wings, and on a hybrid RANS/LES approach. In: C. Liu and Z. Liu, Editors, Advances in DNS/LES, Greyden Press, Columbus, OH (1997).

[10] Delayed DES (DDES)

[11] Spalart et al., 2006 P. Spalart, S. Deck, M. Shur, K. Squires, M. Strelets and A. Travin, A new version of detached-eddy simulation, resistant to ambiguous grid densities, Theor. Comput. Fluid Dyn. 20 (3) (2006), pp. 181–195

[12] Mahjoub, S. N. (2002). Etude de la diffusion d'un panache issu d'une cheminée: application a la maîtrise de la dispersion d'un polluant. Thèse de Doctorat, Ecole Nationale d'Ingénieurs de Monastir, 171.

[13] Schieste, R. (1993). Modélisation et simulation des écoulements turbulents. Hermès, Paris.

[14] Patankar S. V., 1980, Numerical Heat Transfer and Fluid Flow, series in computational methods in mechanics and thermal sciences

[15] Baker, C.J., "The Laminar Horseshoe Vortex," Journal of Fluid Mechanics, Vol. 95, No. 2, pp. 347-367, 1979.

[16] V. Mariotti, S. Camarri, M.V. Savetti, B. Koobus, A. Dervieux, H. Guillard, S. Wornom, Numerical simulation of a jet in crossflow, RR N°5638, Juillet 2005